Global distribution of electrostatic electron cyclotron harmonic waves observed on THEMIS

Binbin Ni,[1] Richard Thorne,[1] Jun Liang,[2] Vassilis Angelopoulos,[3,4] Chris Cully,[5] Wen Li,[1] Xiaojia Zhang,[4] Michael Hartinger,[4] Olivier Le Contel,[6] and Alain Roux[7]

[1] A global, statistical analysis of electrostatic electron cyclotron harmonic (ECH) waves is performed using THEMIS wave data. Our results confirm the high occurrence of <1 mV/m ECH emissions throughout the outer magnetosphere ($L > 5$). The strongest (≥ 1 mV/m) ECH waves are enhanced during geomagnetically disturbed periods, and are mainly confined close to the magnetic equator ($|\lambda| < 3°$) over the region $L \leq 10$ in the night and dawn MLT sector. ECH wave intensities within $3° \leq |\lambda| < 6°$ are generally much weaker but not negligible especially for $L < \sim12$ on the midnight side. Furthermore, the occurrence rates and variability of moderately intense (≥ 0.1 mV/m) ECH emissions suggest that ECH wave scattering could contribute to diffuse auroral precipitation in the outer ($L > 8$) magnetosphere where chorus emissions are statistically weak. **Citation:** Ni, B., R. Thorne, J. Liang, V. Angelopoulos, C. Cully, W. Li, X. Zhang, M. Hartinger, O. Le Contel, and A. Roux (2011), Global distribution of electrostatic electron cyclotron harmonic waves observed on THEMIS, *Geophys. Res. Lett.*, *38*, L17105, doi:10.1029/2011GL048793.

1. Introduction

[2] Electrostatic electron cyclotron harmonic (ECH) emissions occur within bands between the harmonics of electron gyrofrequency, f_{ce}, with dominant frequencies often located around odd half multiples of f_{ce} [e.g., *Kennel et al.*, 1970; *Meredith et al.*, 2009]. These waves propagate at very large angles with respect to the ambient magnetic field [e.g., *Gurnett and Bhattacharjee*, 2005]. Generally, ECH waves are thought to be excited outside the plasmasphere near the geomagnetic equator due to a loss cone instability of electron velocity distribution [e.g., *Ashour-Abdalla and Kennel*, 1978; *Horne et al.*, 2003].

[3] Since the first report of ECH waves by *Kennel et al.* [1970] from the OGO-5 measurements, it has been pro-posed that ECH emissions could act as a viable candidate contributing to diffuse auroral electron precipitation and the magnetic local time (MLT) distribution of plasma sheet electrons in space [e.g., *Kennel et al.*, 1970; *Horne and Thorne*, 2000; *Horne et al.*, 2003]. Recent theoretical and modeling studies [*Thorne et al.*, 2010; *Ni et al.*, 2011a, 2011b] have concluded that whistler-mode chorus waves rather than ECH waves play the dominant role in driving diffuse auroral precipitation in the inner magnetosphere ($<\sim8$ R_e). However, since ECH emissions were reported to extend to $>\sim12$ R_e [e.g., *Roeder and Koons*, 1989], while chorus waves are generally weak (less than a few pT) above ~8 R_e in the night-to-dawn MLT sector [*Li et al.*, 2009], ECH emissions could still be potentially important for understanding the occurrence of nightside diffuse auroral precipitation at higher L-shells [*Newell et al.*, 2009]. Improved information of the global distribution of ECH waves are required to quantify this.

[4] *Kennel et al.* [1970] reported very large amplitude ECH waves, typically between 1 and 10 mV/m and occasionally up to 100 mV/m, using OGO-5 data. Subsequently, *Belmont et al.* [1983] concluded that ECH wave activity was generally more modest based on a statistical analysis of the GEOS-2 data within the 22 - 06 MLT sector and 3° of the magnetic equator, and showed that >1 mV/m ECH events occur less than 2% of the time, compared to 88% occurrence of <0.1 mV/m electric field. A later statistical study by *Roeder and Koons* [1989] of plasma wave data from the AMPTE IRM and SCATHA satellites indicated that the occurrence of ECH wave emissions is comparable to that reported by *Belmont et al.* [1983] and that ECH emissions are observed most often in the 03 - 06 local time (LT) sector of the magnetosphere at geocentric distances of 4 - 8 R_e, confined to $\pm10°$ off the magnetic equator. The work of *Roeder and Koons* [1989] covered a broad L-shell range (4–20) and most local times, but only four equal L-shell bins and eight evenly spaced local time bins were adopted. In addition, their analysis was restricted to a single magnetic dipole latitude bin between $\pm10°$. A recent study by *Meredith et al.* [2009], using CRRES wave data, demonstrated that during active periods strong ECH waves with amplitudes >1 mV/m were observed in the region $4 < L < 7$ from 21 to 06 MLT approximately 20% of the time. However, the CRRES data coverage is mostly confined within 7 R_e with a pronounced gap in the pre-noon sector for $L > 5$.

[5] In the present study we use THEMIS (Time History of Events and Macroscale Interactions during Substorms) wave data to examine the global distribution of averaged ECH electric field amplitude and its occurrence rate as a function of L-shell, MLT, magnetic latitude, and geomagnetic activity level. Directed towards the development of an improved

[1]Department of Atmospheric and Oceanic Sciences, University of California, Los Angeles, California, USA.

[2]Department of Physics and Astronomy, University of Calgary, Calgary, Alberta, Canada.

[3]Institute of Geophysics and Planetary Physics, University of California, Los Angeles, California, USA.

[4]Earth and Space Sciences Department, University of California, Los Angeles, California, USA.

[5]Swedish Institute of Space Physics, Uppsala, Sweden.

[6]Laboratoire de Physique des Plasmas, CNRS/Ecole Polytechnique/UPMC/Paris-Sud 11, St Maur-des-Fossés, France.

[7]Laboratoire de Physique des Plasmas, CNRS/Ecole Polytechnique/UPMC/Paris-Sud 11, Palaiseau, France.

global model for the distribution of ECH waves in the outer magnetosphere (5 to 15 R_e), our analysis not only provides complementary information to earlier studies, but also presents a detailed latitudinal and radial-MLT distribution of ECH emissions under different geomagnetic conditions, which is critical for subsequent theoretical modeling of the role of ECH waves in driving diffuse auroral precipitation.

2. THEMIS Data Analysis

[6] Wave observations from each of the five THEMIS spacecraft [*Angelopoulos*, 2008] come from two instruments, the Electric Field Instrument (EFI) [*Bonnell et al.*, 2008] and the Search Coil magnetometer (SCM) [*Roux et al.*, 2008; *Le Contel et al.*, 2008] that measure the wave electric and magnetic field components in three directions respectively. Based on the THEMIS EFI and SCM measurements, two spectral datasets are produced: the Filter Bank (FBK) and Fast Fourier Transform (FFT). This study uses the FBK electric and magnetic field data, calculated from the Digital Fields Board (DFB) [*Cully et al.*, 2008], to represent the mean amplitude of the electric and magnetic field of the bandpass-filtered signals from the spin-plane EFI and SCM sensors in 6 logarithmically-spaced frequency bands from 0.1 Hz to 4 kHz, with a measurement cadence of 4 seconds. We analyze the FBK data from 1 January 2008 to December 31 2009 for all 5 probes. With the available solar wind data and geomagnetic indices, the Tsyganenko 96 (T96) magnetic field model [*Tsyganenko and Stern*, 1996] is adopted to map data to the magnetic equator to obtain L, MLT and magnetic latitude (λ) where each observation occurred using the ONERA-DESP library V4.2. All points within the L range of 5 - 15 and the magnetic latitude range $|\lambda| < 10°$ are selected for the following wave investigation.

[7] Our selection criteria for ECH wave events are as follows:

[8] 1. We first exclude data points with observed ion velocity >50 km/s and electron total temperature <200 eV to avoid events possibly outside the magnetopause. Besides isolating the EFI sphere shadowing periods (several weeks per year per probe), we select data with spacecraft potentials <70 volts to eliminate events either in the Earth shadow region or in the lobes where large uncertainties in wave measurements often occur. Since ECH waves are usually located near the equator, we focus on data with $B_z > \sqrt{B_x^2 + B_y^2}$ (where B_x, B_y, and B_z are the three components of ambient magnetic field in the GSM coordinates). This also guarantees a relatively small angle between the ambient magnetic field and the satellite spin axis to ensure that a substantial component of the electric/magnetic wave field can be recorded by spin-plane sensor and registered in the FBK data.

[9] 2. The background magnetic field measured from the THEMIS Flux-Gate Magnetometer (FGM) [*Auster et al.*, 2008] and the probe magnetic latitude inferred from the T96 model are used to calculate the equatorial magnetic field strength and f_{ce}, which is subsequently adopted to evaluate the harmonic band of ECH waves. The six FBK bands are denoted as FBK #1 to FBK #6, from low to high frequencies, covering the frequency range of 1 to 4 Hz, 5 to 14 Hz, 20 to 57 Hz, 80 to 227 Hz, 316 to 904 Hz, and 1390 to 4000 Hz, respectively. Since ECH waves are narrow-band emissions,

with the major power intensities commonly located above $(n+0.2) f_{ce}$ particularly for the first three harmonic bands [e.g., *Meredith et al.*, 2009; *Ni et al.*, 2011a], we take the upper-cutoff frequency of each FBK band divided by a factor of 1.2 as the threshold frequencies to differentiate ECH wave bands. Specifically, there are seven cases under consideration: (I) when $f_{ce} \geq 3333$ Hz (= 4000 Hz/1.2), there is no data at ECH frequencies available; (II) when 753 Hz (= 904 Hz/1.2) $\leq f_{ce} < 3333$ Hz, only FBK #6 lies in the ECH frequency range, including the first harmonic and possibly higher harmonics dependent on the value of f_{ce}; (III) when 189 Hz (= 227 Hz/1.2) $\leq f_{ce} < 753$ Hz, FBK #5 and #6 are in the ECH frequency range, but only FBK #5 covers the first harmonic band; (IV) when 48 Hz (= 57 Hz/1.2) $\leq f_{ce} < 189$ Hz, FBK #4 - #6 are in the ECH frequency range, but only FBK #4 covers the first harmonic band; (V) when 12 Hz (= 14 Hz/1.2) $\leq f_{ce} < 48$ Hz, FBK #3 - #6 are in the ECH frequency range, but only FBK #3 covers the first harmonic band; (VI) when 3.3 Hz (= 4 Hz/1.2) $\leq f_{ce} < 12$ Hz, FBK #2 - #6 are in the ECH frequency range, but only FBK #2 covers the first harmonic band; and (VII) when $f_{ce} < 3.3$ Hz, all the FBK bands are in the ECH frequency range, but only FBK #1 covers the first harmonic band.

[10] 3. For each wave event identified above, we select only the wave data for the FBK band including the first ECH harmonic band that is most intense among all the observable ECH harmonic bands. Taking into account the electrostatic nature of ECH emissions, we remove events with the recorded magnetic field amplitude >4 pT. We note that the EFI noise floor exists for each FBK frequency band and that the ~0.02 – 0.03 mV/m signals can be strongly contaminated by the shot noise on the probes in the highest-frequency bands. Although the signals <0.03 mV/m cannot be discerned above the instrument noise and thus become unreliable, we conservatively include them as zero values for analysis of the mean amplitude of the geophysical waves.

[11] After performing the above procedure and multiplying the raw FBK electric field value by a factor $\pi/2$ to convert it into the nominal wave amplitude, we establish a robust database for well-determined ECH wave events, covering a two-year period for all five THEMIS probes, for the subsequent statistical analysis.

3. Statistical Results

3.1. Global Distribution of ECH Waves Under Different Geomagnetic Activities

[12] To investigate the dependence of ECH wave power on the level of geomagnetic activity, we adopt AE* (the mean value of AE index in the previous hour) to separate all identified ECH wave events into three categories of geomagnetic condition: quiet (AE* < 100 nT), moderate (100 nT $\leq$ AE* $\leq$ 300 nT), and active (AE* > 300 nT). The corresponding THEMIS FBK electric field amplitude data are then binned as a function of L in steps of 0.5 L and MLT with an interval of one hour. To examine the latitudinal variation of ECH wave power, we divide the considered magnetic latitudes ($|\lambda| < 10°$) into three magnetic latitude intervals: $|\lambda| < 3°$, $3° \leq |\lambda| < 6°$, and $6° \leq |\lambda| < 10°$.

[13] Figure 1 shows the average root-mean-square (RMS) ECH wave electric field amplitude (E_w) and the number of total samples in each bin as a function of L-shell and MLT for the indicated three geomagnetic conditions and three
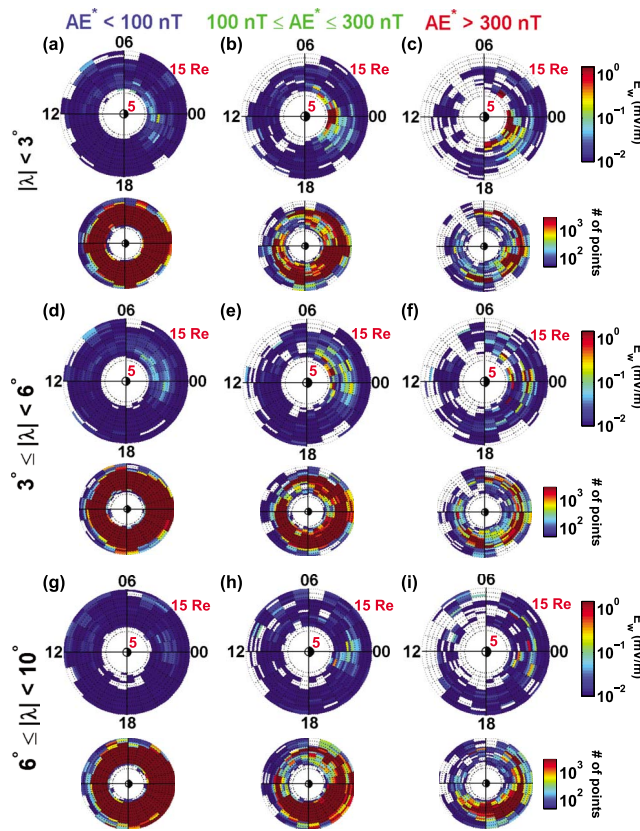
Figure 1. Global distribution of ECH waves as a function of L-shell and MLT under different geomagnetic conditions categorized by AE* (from left to right: quiet, moderate, and active) for three specified magnetic latitude intervals: (a, b, c) $|\lambda| < 3°$, (d, e, f) $3° \leq |\lambda| < 6°$, and (g, h, i) $6° \leq |\lambda| < 10°$. The larger plots show the root-mean-square ECH wave electric field amplitudes E_w (in units of mV/m) and the smaller plots indicate the number of total samples in each bin.

magnetic latitude intervals. The large panels represent the global distribution of E_w and the smaller panels represent the number of total samples. The number of samples at L > 12 is much smaller than that at lower L-shells since the samples at L > 12 are collected from only THEMIS B and C. To pursue a better resolution at the lower sampling periods where the waves are more pronounced, we have allowed saturation for high sampling ($>10^4$) to bring out the important features for the more intense waves. It is evident that stronger ECH waves (≥ 0.1 mV/m) generally occur in the $\sim 21 - 06$ MLT sector and extend from L = 5 to L ≥ 10 with the presence of most intense emissions within L = 5 − 9, qualitatively consistent with *Roeder and Koons* [1989] and *Meredith et al.* [2009] (in the overlap region of L = 5−7 for the latter). Compared to quiet periods, ECH waves intensify significantly and cover a broader (L, MLT) range during enhanced geomagnetic activity. The difference in E_w distribution between moderate and active conditions is also noticeable, showing a solid MLT peak occurrence at premidnight or near midnight during active periods. Besides the pronounced L-MLT and geomagnetic activity dependence of E_w, there is a distinct latitudinal dependence of E_w. In good agreement with the previous studies [e.g., *Roeder and Koons*, 1989; *Meredith*

et al., 2009], ECH waves observed on THEMIS are well confined to within $|\lambda| < 6°$. At higher latitudes ECH emissions are extremely weak even when AE* > 300 nT. There also exists a tendency of a systematic shift in ECH wave occurrence and intensity with magnetic latitude. Equatorial emissions are most frequently observed at premidnight, while waves >3° are more likely present at post midnight. While the strongest ECH waves (≥ 1 mV/m) are characteristically present within 3° of the magnetic equator, the wave activity within $3° \leq |\lambda| < 6°$ is well above the noise level and ≥ 1 mV/m ECH waves can extend to L-shell up to ~12, especially within $23 - 04$ MLT. These amplitude features are consistent with Figure 3 of *Meredith et al.* [2009] within $|\lambda| < 3°$ at L = 5−7. The E_w values are obtained using the four-second averaged FBK data, whereas the instantaneous wave amplitudes can greatly exceed these 4-second averages, e.g., as reported by *Liang et al.* [2010] using the THEMIS wave burst mode data.

3.2. Global Occurrence of ECH Waves Under Different Levels of Wave Amplitude

[14] To investigate the global occurrence pattern of ECH waves, the wave electric field data is sorted into three different levels of wave electric field amplitude: relatively weak (0.03 - 0.1 mV/m), moderate (0.1 - 1 mV/m), and strong (≥ 1 mV/m). To determine the occurrence rates of ECH emissions associated with different wave amplitude levels, we compute the ratio of the number of samples, whose corresponding E_w are located in the assigned ECH wave amplitude level, to the number of total samples in each spatial bin.

[15] Figure 2 shows the occurrence rates of different levels of ECH wave amplitude within $|\lambda| < 3°$ as a function of L, MLT, and geomagnetic activity level. 0.03–0.1 mV/m ECH
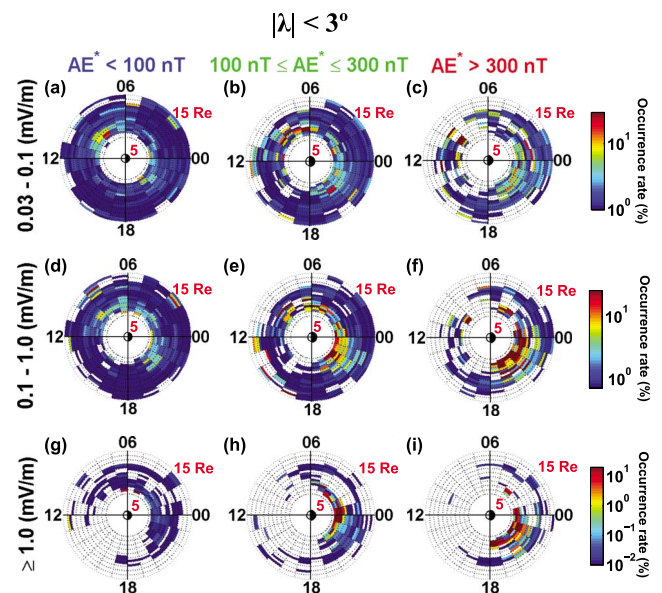
Figure 2. Global occurrence rates of ECH waves within $|\lambda| < 3°$ under different geomagnetic conditions (from left to right: quiet, moderate, and active) for three different wave amplitude levels: (a, b, c) relatively weak with 0.03 mV/m $\leq E_w < 0.1$ mV/m, (d, e, f) moderate with 0.1 mV/m $\leq E_w < 1$ mV/m, and (g, h, i) strong with $E_w \geq 1$ mV/m.
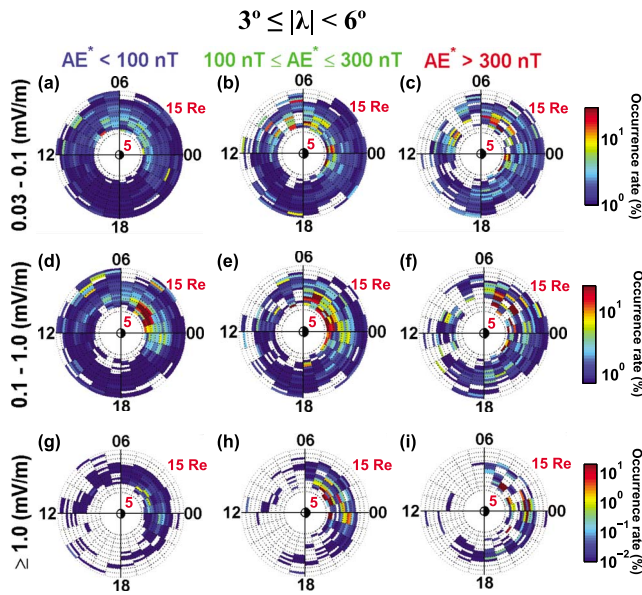
Figure 3. Same as in Figure 2, except for ECH waves within $3° \leq |\lambda| < 6°$.

waves are present with a broad (L, MLT) coverage. The occurrence is commonly at a rate of a few percent, whereas varying from 1% to > 30% with the peak at $L \leq 10$ on the midnight-to-postdawn side. The occurrences of both moderate (row 2) and strong (row 3) ECH waves indicate a clear trend of expansion of wave activity to higher L-shells with enhanced occurrences when geomagnetic activity intensifies, with the highest rates found between $L = 5–10$ in the night and dawn sectors. The occurrence rates vary from below 1% during quiet times to up to ~40% during disturbed periods for moderate waves, and from <0.1% during quiet times to ~20% during disturbed times for strong waves. Especially for $AE^* > 300$ nT, ≥ 1 mV/m ECH waves show a distinct absence on the dayside but an average occurrence rate at a few percent or above within $L \sim 9$ on the nightside. The obtained overall pattern of ECH wave occurrence confirms a high occurrence of <1 mV/m ECH waves in the magnetosphere. It agrees well with the results of *Meredith et al.* [2009] over the overlap region of $L = 5–7$, especially on the nightside where the CRRES statistics is good. Additionally, our results are qualitatively consistent with the lower resolution analysis of *Roeder and Koons* [1989] for ECH waves of spectral density >1 μV/m/Hz$^{1/2}$ within $|\lambda| < 10°$.

[16] Figure 3 represents the global occurrence pattern of ECH emissions at different wave amplitude levels for $3° \leq |\lambda| < 6°$. Similar to the results in Figure 2, the occurrence rates exhibit a strong dependence on L, MLT, geomagnetic activity level, and amplitude level. Specifically, 0.03–0.1 mV/m ECH emissions exhibit relatively high occurrence rates up to ~40% on the night and dawn side, dependent on geomagnetic condition. More intense ECH waves exhibit a pronounced dawn-dusk asymmetry with the strongest waves occurring in the 23 – 04 MLT sector at L-shells of 5–10 with a rate below ~30%. Even though the occurrence rates of intense ECH waves for $3° \leq |\lambda| < 6°$ are similar to those for $|\lambda| < 3°$, the E_w values are weaker at higher latitudes, presumably due to ECH wave damping during propagation away from the source region to higher latitudes. Furthermore, intense ECH waves within $3° \leq |\lambda| < 6°$ tend to occur more often at higher

L-shells and later MLT, possibly owing to radial and azimuthal wave propagation effects.

4. Summary and Discussion

[17] We have utilized two years of filter bank data obtained on all five THEMIS probes to perform an improved statistical survey of the global distribution of ECH waves in the Earth's magnetosphere. Complementary to previous statistical analyses on ECH waves [*Belmont et al.*, 1983; *Roeder and Koons*, 1989; *Meredith et al.*, 2009], our investigation covers a broad radial L range of 5 to 15 at magnetic latitudes $|\lambda| < 10°$ and all magnetic local times, with high resolution in both L-shell and MLT. Directed towards the development of an improved global model for the distribution of ECH emissions and the occurrence pattern of wave strength as a function of L-shell, MLT, and magnetic latitude under different geomagnetic conditions, our main results are summarized as follows:

[18] 1. The intensity of ECH emissions is strongly L-shell dependent with a pronounced MLT asymmetry. More intense ECH waves, with RMS amplitudes ≥ 0.1 mV/m, are typically confined within $L = 5–10$ in the night and dawn sectors (~21 – 06 MLT). ECH waves are usually much weaker for the other (MLT, L) locations.

[19] 2. The RMS amplitude of ECH waves intensifies considerably during enhanced geomagnetic activity, compared to that for quiet periods ($AE^* < 100$ nT). Active-time ECH wave activity shows a solid MLT peak occurrence at premidnight or near midnight.

[20] 3. Strongest ECH emissions are characteristically present within $|\lambda| < 3°$, in good agreement with previous analyses. ECH waves within $3° \leq |\lambda| < 6°$ are comparatively weaker but still well above the noise level, especially for $L = 5 – ~12$ near midnight.

[21] 4. ECH emissions show a clear expansion to higher L-shells with enhanced occurrences when geomagnetic activity intensifies. Relatively weak (0.03–0.1 mV/m) ECH waves exhibit an occurrence rate up to ~40%. The occurrence rates of moderate (0.1–1 mV/m) and strong (≥ 1 mV/m) ECH waves have a pronounced MLT asymmetry, varying from <1% during quiet times to >~30% during disturbed periods with highest occurrences on the night-to-dawn side within $L = 5–10$. The global occurrence patterns of ECH waves at different amplitude levels are similar for the intervals of $|\lambda| < 3°$ and $3° \leq |\lambda| < 6°$.

[22] A comparison between geomagnetic activity and the occurrence frequency of ECH waves under different wave amplitude levels revealed in this study suggests that triggering of ECH waves does not necessarily require dramatic intensification of geomagnetic activity, supporting the idea that a loss cone distribution (which is present under most circumstances) is the major mechanism for ECH wave generation. However, the disturbed conditions associated with enhanced convection and/or substorm activity very likely lead to preferential ECH wave amplification, as a consequence of increased free energy in the electron loss cone distribution, but such enhanced excitation requires detailed theoretical investigation in future studies.

[23] While ECH wave scattering has been concluded to be much less influential than whistler-mode chorus scattering for diffuse auroral precipitation in the inner magnetosphere [*Thorne et al.*, 2010; *Ni et al.*, 2011a, 2011b], our reported statistical results suggest that ECH wave scattering could be

important for diffuse auroral precipitation outside $L \approx 8$ where chorus activities are statistically much weaker [*Li et al.*, 2009]. Although the strongest ECH emissions with $E_w \geq$ 1 mV/m are most likely to occur within the region L = 5–10, more moderate ECH emissions with E_w of the order of 0.1 mV/m are still capable of scattering plasma sheet electrons at a rate comparable to the strong diffusion limit at higher L-shells, because the strong diffusion rate decreases substantially with a smaller loss cone and a longer bounce period. To fully understand the role of ECH waves in the global morphology of diffuse auroral precipitation in the non-dipolar magnetic field environment of the outer magnetosphere ($L \geq 8$) requires detailed quantitative evaluation of ECH wave induced diffuse auroral scattering rates. This can be accomplished in the near future using the improved global ECH wave model presented above, together with the frequency spectrum of ECH wave power obtained from THEMIS high-resolution wave burst mode data and the wave normal angle distribution of multi-banded ECH emissions obtained from detailed ray tracing studies.

References

Angelopoulos, V. (2008), The THEMIS mission, *Space Sci. Rev.*, *141*, 5–34, doi:10.1007/s11214-008-9336-1.

Ashour-Abdalla, M., and C. F. Kennel (1978), Nonconvective and convective electron cyclotron harmonic instabilities, *J. Geophys. Res.*, *83*, 1531–1543, doi:10.1029/JA083iA04p01531.

Auster, U., et al. (2008), The THEMIS fluxgate magnetometer, *Space Sci. Rev.*, *141*, 235–264, doi:10.1007/s11214-008-9365-9.

Belmont, G., D. Fontaine, and P. Canu (1983), Are equatorial electron cyclotron waves responsible for diffuse auroral electron precipitation?, *J. Geophys. Res.*, *88*, 9163–9170, doi:10.1029/JA088iA11p09163.

Bonnell, J. W., et al. (2008), The electric field instrument (EFI) for THEMIS, *Space Sci. Rev.*, *141*, 303–341, doi:10.1007/s11214-008-9469-2.

Cully, C. M., R. E. Ergun, K. Stevens, A. Nammari, and J. Westfall (2008), The THEMIS digital fields board, *Space Sci. Rev.*, *141*, 343–355, doi:10.1007/s11214-008-9417-1.

Gurnett, D. A., and A. Bhattacharjee (2005), *Introduction to Plasma Physics: With Space and Laboratory Applications*, Cambridge Univ. Press, Cambridge, U. K.

Horne, R. B., and R. M. Thorne (2000), Electron pitch angle diffusion by electrostatic electron cyclotron harmonic waves: The origin of pancake distributions, *J. Geophys. Res.*, *105*, 5391–5402, doi:10.1029/1999JA900447.

Horne, R. B., R. M. Thorne, N. P. Meredith, and R. R. Anderson (2003), Diffuse auroral electron scattering by electron cyclotron harmonic and whistler mode waves during an isolated substorm, *J. Geophys. Res.*, *108*(A7), 1290, doi:10.1029/2002JA009736.

Kennel, C. F., F. L. Scarf, R. W. Fredricks, J. H. McGehee, and F. V. Coroniti (1970), VLF electric field observations in the magnetosphere, *J. Geophys. Res.*, *75*, 6136–6152, doi:10.1029/JA075i031p06136.

Le Contel, O., et al. (2008), First results of the THEMIS searchcoil magnetometers, *Space Sci. Rev.*, *141*, 509–534, doi:10.1007/s11214-008-9371-y.

Li, W., R. M. Thorne, V. Angelopoulos, J. Bortnik, C. M. Cully, B. Ni, O. Le Contel, A. Roux, U. Auster, and W. Magnes (2009), Global distribution of whistler-mode chorus waves observed on the THEMIS spacecraft, *Geophys. Res. Lett.*, *36*, L09104, doi:10.1029/2009GL037595.

Liang, J., V. Uritsky, E. Donovan, B. Ni, E. Spanswick, T. Trondsen, J. Bonnell, A. Roux, U. Auster, and D. Larson (2010), THEMIS observations of electron cyclotron harmonic emissions, ULF waves, and pulsating auroras, *J. Geophys. Res.*, *115*, A10235, doi:10.1029/2009JA015148.

Meredith, N. P., R. B. Horne, R. M. Thorne, and R. R. Anderson (2009), Survey of upper band chorus and ECH waves: Implications for the diffuse aurora, *J. Geophys. Res.*, *114*, A07218, doi:10.1029/2009JA014230.

Newell, P. T., T. Sotirelis, and S. Wing (2009), Diffuse, monoenergetic, and broadband aurora: The global precipitation budget, *J. Geophys. Res.*, *114*, A09207, doi:10.1029/2009JA014326.

Ni, B., R. M. Thorne, R. B. Horne, N. P. Meredith, Y. Y. Shprits, L. Chen, and W. Li (2011a), Resonant scattering of plasma sheet electrons leading to diffuse auroral precipitation: 1. Evaluation for electrostatic electron cyclotron harmonic waves, *J. Geophys. Res.*, *116*, A04218, doi:10.1029/2010JA016232.

Ni, B., R. M. Thorne, N. P. Meredith, R. B. Horne, and Y. Y. Shprits (2011b), Resonant scattering of plasma sheet electrons leading to diffuse auroral precipitation: 2. Evaluation for whistler mode chorus waves, *J. Geophys. Res.*, *116*, A04219, doi:10.1029/2010JA016233.

Roeder, J. L., and H. C. Koons (1989), A survey of electron cyclotron waves in the magnetosphere and the diffuse auroral electron precipitation, *J. Geophys. Res.*, *94*, 2529–2541, doi:10.1029/JA094iA03p02529.

Roux, A., O. Le Contel, C. Coillot, A. Bouabdellah, B. de la Porte, D. Alison, S. Ruocco, and M. C. Vassal (2008), The search coil magnetometer for THEMIS, *Space Sci. Rev.*, *141*, 265–275, doi:10.1007/s11214-008-9455-8.

Thorne, R. M., B. Ni, X. Tao, R. B. Horne, and N. P. Meredith (2010), Scattering by chorus waves as the dominant cause of diffuse auroral precipitation, *Nature*, *467*, 943–946, doi:10.1038/nature09467.

Tsyganenko, N., and D. Stern (1996), Modeling the global magnetic field of the large-scale Birkeland current systems, *J. Geophys. Res.*, *101*, 27,187–27,198, doi:10.1029/96JA02735.

V. Angelopoulos, Institute of Geophysics and Planetary Physics, University of California, 3845 Slichter Hall, Los Angeles, CA 90095-1567, USA.

C. Cully, Swedish Institute of Space Physics, Box 537, SE-75121 Uppsala, Sweden.

M. Hartinger and X. Zhang, Earth and Space Sciences Department, University of California, 603 Charles E. Young Dr. E., Los Angeles, CA 90095, USA.

O. Le Contel, Laboratoire de Physique des Plasmas, CNRS/Ecole Polytechnique/UPMC/Paris-Sud 11, 4, avenue de Neptune, F-94107 St Maur-des-Fossés CEDEX, France.

W. Li, B. Ni, and R. Thorne, Department of Atmospheric and Oceanic Sciences, University of California, 405 Hilgard Ave., Los Angeles, CA 90095-1565, USA.

J. Liang, Department of Physics and Astronomy, University of Calgary, 2500 University Dr., Calgary, AB T2N 1N4, Canada.

A. Roux, Laboratoire de Physique des Plasmas, CNRS/Ecole Polytechnique/UPMC/Paris-Sud 11, route de Saclay, F-91128 Palaiseau CEDEX, France.